Supplementary Materials

Exploring performance degradation of quantum-dot light-emitting diodes

Aqiang Liu, Chunyan Cheng, Jianjun Tian*

Institute for Advanced Materials and Technology, University of Science and Technology Beijing, Beijing 100083, P. R. China

*Email: tianjianjun@mater.ustb.edu.cn

Experimental Methods

Materials

PEDOT:PSS (Baytron PVP Al 4083) and TFB (Molecular weight ~85000) were purchased Xi'an Polymer Light Technology Corp. QDs (CdSe/ZnS core-shell) was purchased Suzhou Xingshuo Nanotech Co. Ltd. Solvent, chlorobenzene (99.8%), ethyl acetate (99.5%), Dimethyl sulfoxide (DMSO) and ethanol (99.8%) were purchased Aladdin. All chemical reagents were used directly without further purification.

Preparation of ZnMgO nanocrystals. ZnMgO nanocrystals were synthesized by previously reported methods.[1] Concretely, $Zn(Ac)_2 \cdot 2H_2O$ (296 mg) and $Mg(Ac)_2 \cdot 4H_2O$ (32 mg) were dissolved in DMSO (15 mL) and then added a 5 mL ethanol solution containing TMAH (343 mg). The mixed solution was stirred at 25 ℃ for 1 h. The ZnMgO nanocrystals were collected by adding excess ethyl acetate and centrifugation. Finally, the collected ZnMgO nanocrystals were dispersed into ethanol solution (20 mg L^{-1}).

Device fabrication. Deionized water, acetone, and ethanol were successively used for ultrasonic cleaning of patterned ITO conductive glasses. The cleaned ITO substrates were treated by UV-Ozone cleaner for 20 min. PEDOT:PSS solutions were spin-coated onto the patterned ITO conductive substrates at 3500 rpm for 40 s and annealed at 140

℃ for 15 min. The PEDOT:PSS-coated substrates were transferred to N_2-glovebox for subsequent deposition. The TFB solutions (in chlorobenzene, 12 mg mL^{-1}) were spin-coated onto the PEDOT:PSS-coated substrates at 2500 rpm for 40 s and annealed at 125 ℃ for 30 min. The CdSe/ZnS QDs (in octane, 15 mg mL^{-1}) were spin-coated onto the TFB-coated substrates at 2000 rpm for 40 s. The ZnMgO nanocrystals (in ethanol, 20 mg mL^{-1}) were spin-coated onto the QDs-coated substrates at 2500 rpm for 40 s and annealed at 100 ℃ for 10 min. Finally, about 80 nm Ag electrode was deposited on the ZnMgO layer by thermal evaporation. The thickness of PEDOT:PSS, TFB, QDs, and ZnO are 34 nm, 47 nm, 20 nm, and 31 nm, respectively. For the QLEDs with PMMA insert layer, a PMMA solution (in acetone, 4 mg mL^{-1}) were spin-coated onto the QDs-coated substrates at 4000 rpm for 40 s and annealed at 100 ℃ for 5 min before depositing ZnMgO, the thickness of PMMA is about 6 nm.

Removing ZnMgO and Ag electrodes are critical steps in devices (ITO/PEDOT:PSS/TFB/ZnMgO/Ag) transformed to reconstructed QLEDs or hole-only devices. The removal method refers to the previous literature.[2] The Ag electrode can be easily peeled off by adhesive tapes. ZnMgO nanocrystals were cleaned up by a dilute ethanol solution of acetic acid (0.5% volume ratio), and then washed with ethanol and annealed at 60 °C for 30 min. For reconstructed QLEDs, the QDs, ZnMgO were deposited by spin-coating, and then the Ag electrodes was deposited by thermal evaporation. For hole-only devices, the MoO_3, and Ag electrodes were deposited by thermal evaporation.

Device characterization. The J-V-L cruve, luminance, and EQE of QLEDs were measured with a Keithley 2400 source-meter coupled with a PR-655 Spectra Scan spectrophotometer. The T_{95} operation lifetime of QLEDs was obtained using the same testing system.

Optical characterization. UV-vis absorption spectrum was recorded by a Shimadzu UV-3600 plus spectrophotometer. Steady-state PL spectra were presented by a

Gangdong F-280 fluorescence spectrometer with a 150 W Xe lamp as an excitation source. The PLQYs were obtained by an integrating sphere (Edinburgh, FLS920). Time-resolved PL decay spectra of QDs were recorded by a Horiba Fluorolog spectrometer coupled with a 375 nm, 45 ps pulsed laser and a time-corrected single-photon counting system.

TEM and optical microscopes measurement. The morphology of QDs were recorded by a JEOL JEM-2010 microscope. The EL image of QLEDs and the surface morphology of aged TFB films were present by a GB-15100 optical morphology.

In situ electrical and optical monitoring system. To study the origin of operation instability of QLEDs, an in-situ electrical and optical monitoring system was constructed. The layout of the monitoring system is emerging in **Figure 2a**. A 365 nm laser was used to excite the QLEDs. A Keithley 2400 source-meter was used to provide an electrical signal. The PL and EL spectrum was monitored by a monochromator coupled with a lock-in amplifier.

Electrochemical in situ fluorescence spectroscopy. A electrochemical workstation was used to provide an electrical signal for the electrochemical reduction and oxidation of TFB films. The ITO/TFB film, Pt tablet, and Ag/AgCl electrode were used as working electrode (WE), counter electrode (CE), and reference electrode (RE), respectively. Tetrabutylammonium tetrafluoroborate (10 g) was dissolved in acetonitrile (40 mL) was used as an electrolyte solution (250 mg mL^{-1}). A 365 nm laser together with a photodetector were used to excite and monitor the fluorescence spectrum of the TFB films.

1. The characterization of quantum dots (QDs) used in this work

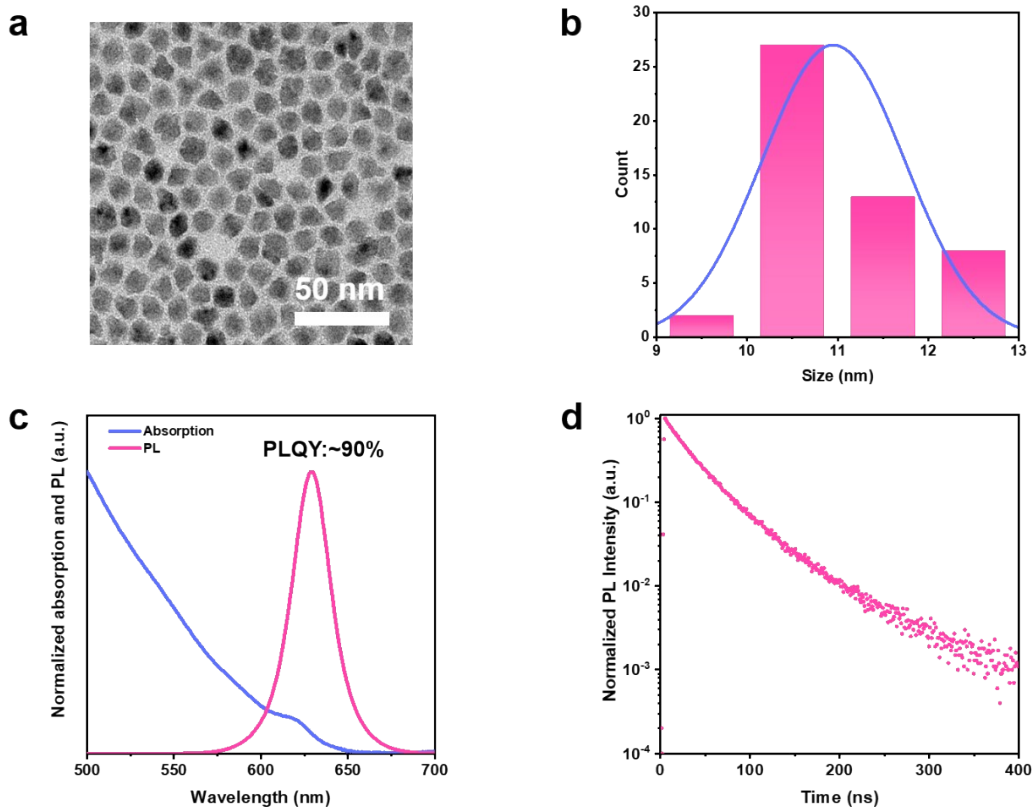

Figure S1. The characterization of QDs used in this work. (a) TEM image. (b) Size distribution of QDs. (c) UV-vis and PL spectrum. (d) Time resolved PL deacy curve.

2. The performance of the QLEDs.

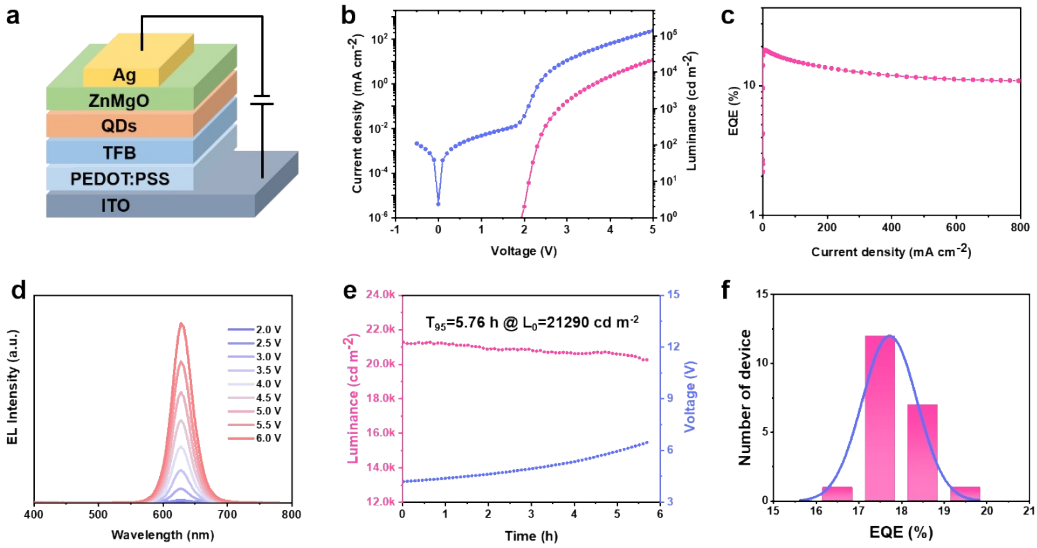

Figure S2. The performance of the QLEDs. (a) Device structure. (b) J-V-L characteristics curve. (c) EQE-J of the QLEDs. (d) EL spectra of the QLEDs at different operating voltages. (e) T_{95} of the QLEDs at an initial luminance of 21,290 cd m-2. (f) Histograms of the EQE.

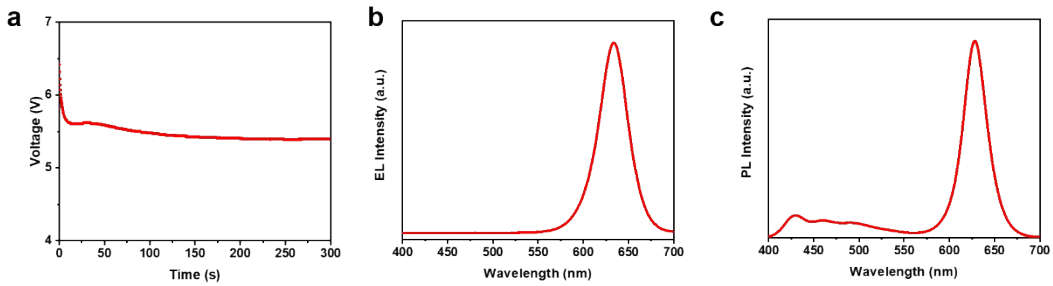

Figure S3. In-situ electrical and optical monitoring system. (a) The V-t curve of QLEDs operating at the constant current. (b) EL spectra of QLEDs operating at the constant current. (c) PL spectra of QLEDs under off-working state.

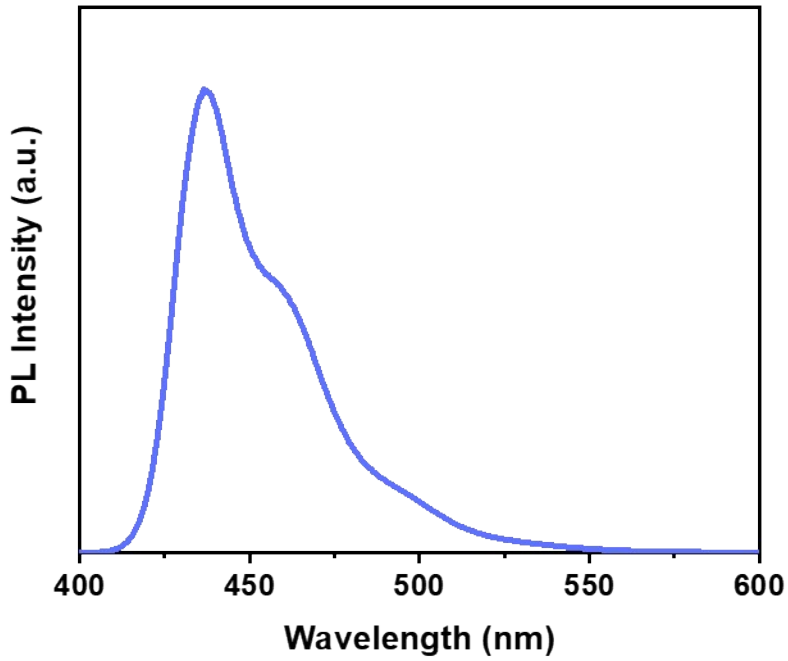

Figure S4. The PL spectra of fresh TFB solution.

3. The simulated equivalent circuit of QLEDs

LED is essentially a p-n junction, and its I-V characteristic curve follows the Shockley equation (1),

$$I = I_s exp\left(\frac{eV}{nkT}\right) \quad (1)$$

Where n and I_s are the ideality factor and saturation current density of the QLED, respectively. KT is roughly equivalent to 26 meV at room temperature. Based on the Shockley equation, it can be seen that there is an exponential relation between current density and applied voltage, which is a linear in semilogarithmic coordinate system (**Figure S4a**).

However, there is inevitable parasitic resistance in QLEDs, such as series resistance (R_s) caused by contact resistance, parallel resistance (R_p) caused by any channel that bypasses the QDs active layer. The existence of parasitic resistances leads to the I-V characteristic curve of QLEDs deviating from the exponential relation and appearing the nonlinear relation in the semilogarithmic coordinate system. Therefore, the Shockley equation must be revised to account for parasitic resistances. Assuming an ideal diode in parallel with a resistance, and then in series with a resistance. the I-V characteristic of diodes is revised to

$$I = \frac{V - IR_s}{R_p} + I_s exp\left(\frac{e\left(V - IR_s\right)}{nkT}\right) \quad (2)$$

If an ideal diode is connected in parallel with resistance, the I-V characteristic curve is present in **Figure S4b**. As a comparison, if an ideal diode is connected in series with resistance, the I-V characteristic curve is shown in **Figure S4c**. In the real world, the ideal diodes, R_p and R_s coexist in QLEDs. **Figure 2d** shows that the I-V characteristic curve of the diodes together with R_p and R_s. Generally, the R_p is much larger than that of the R_s. Therefore, the current is mainly affected by R_p at low bias voltage. Then, the current rapid growth when the voltage increases enough to overcome build-in potential of diodes. Finally, the current is limited by R_s.

Therefore, the equivalent circuit of QLED can be simplified and determined from the IV characteristic curve.

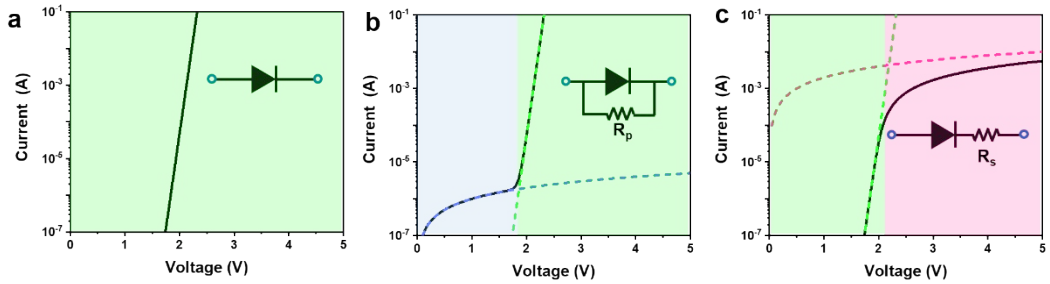

Figure S5. The assessment of equivalent circuit by the IV curve of diodes. (a) I-V characteristic curve of the ideal diode. (b) I-V characteristic curve of the ideal diode with R_p. (c) I-V characteristic curve of the ideal diode with R_s.

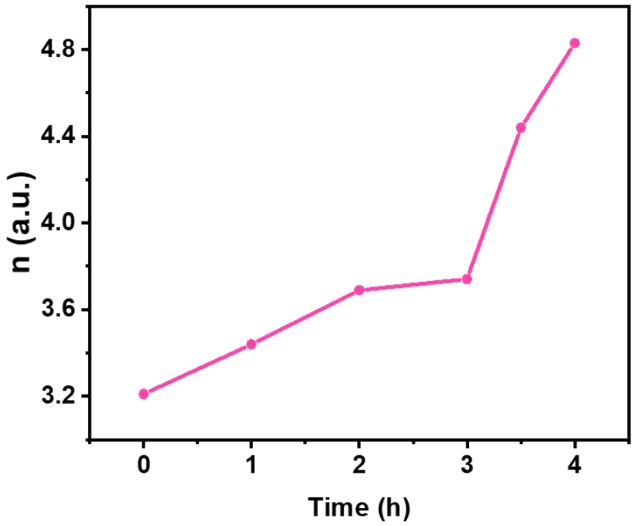

Figure S6. Operation time-dependent traces of the fitted n in the QLEDs.

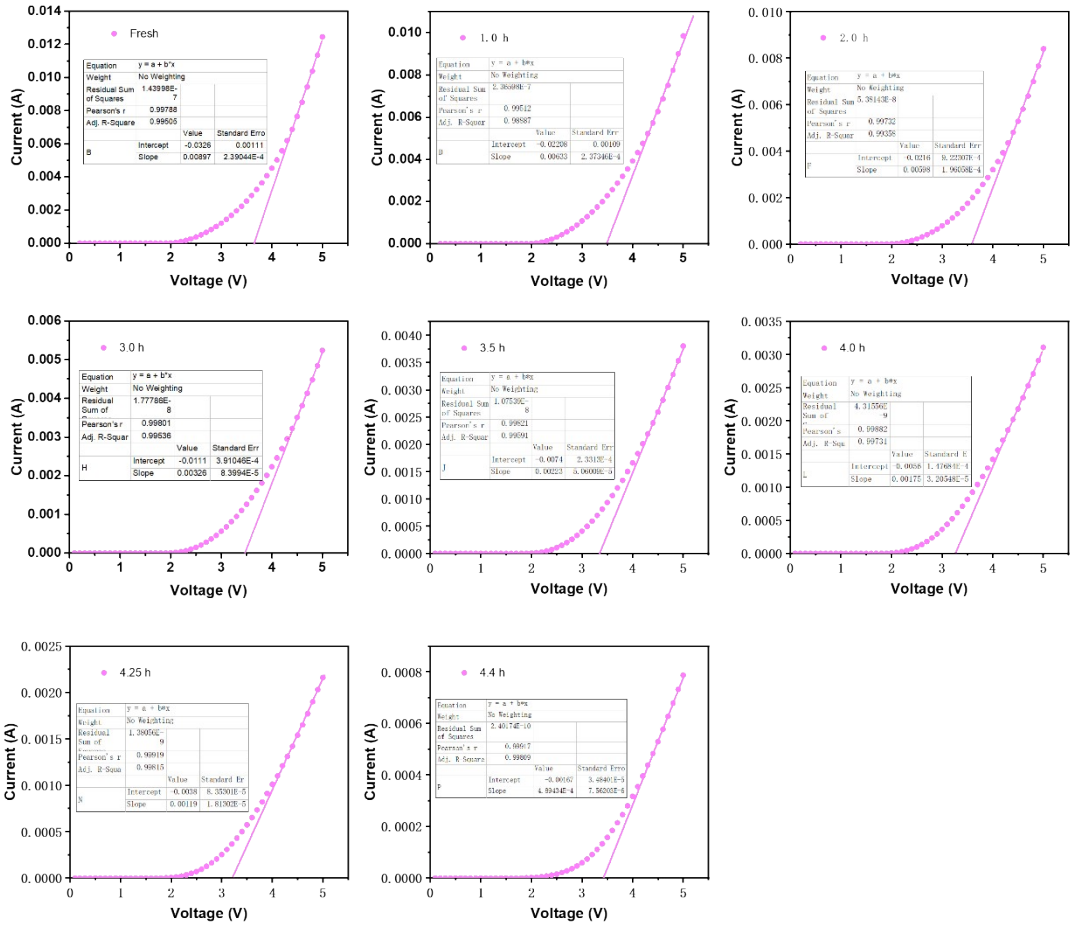

Figure S7. The fitting diagram of R_s.

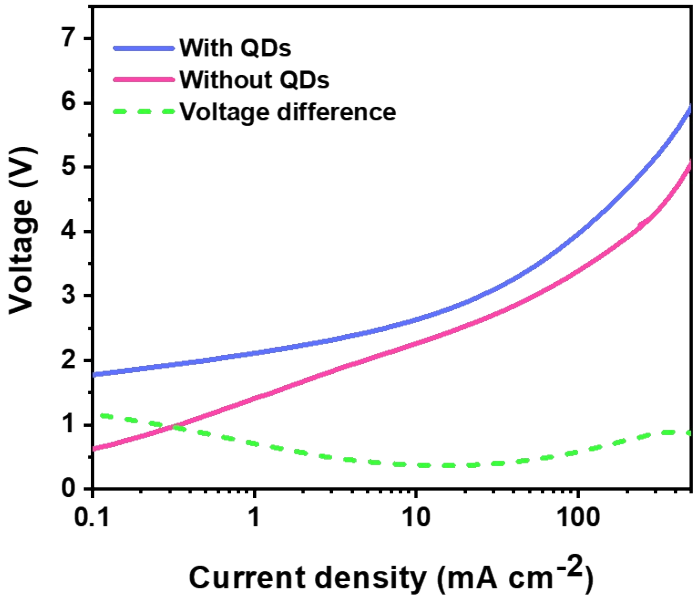

Figure S8. Comparison of V-J characteristic between devices with structures of ITO/PEDOT:PSS/TFB/QDs/ZnMgO/Ag and ITO/PEDOT:PSS/TFB/ZnMgO/Ag.

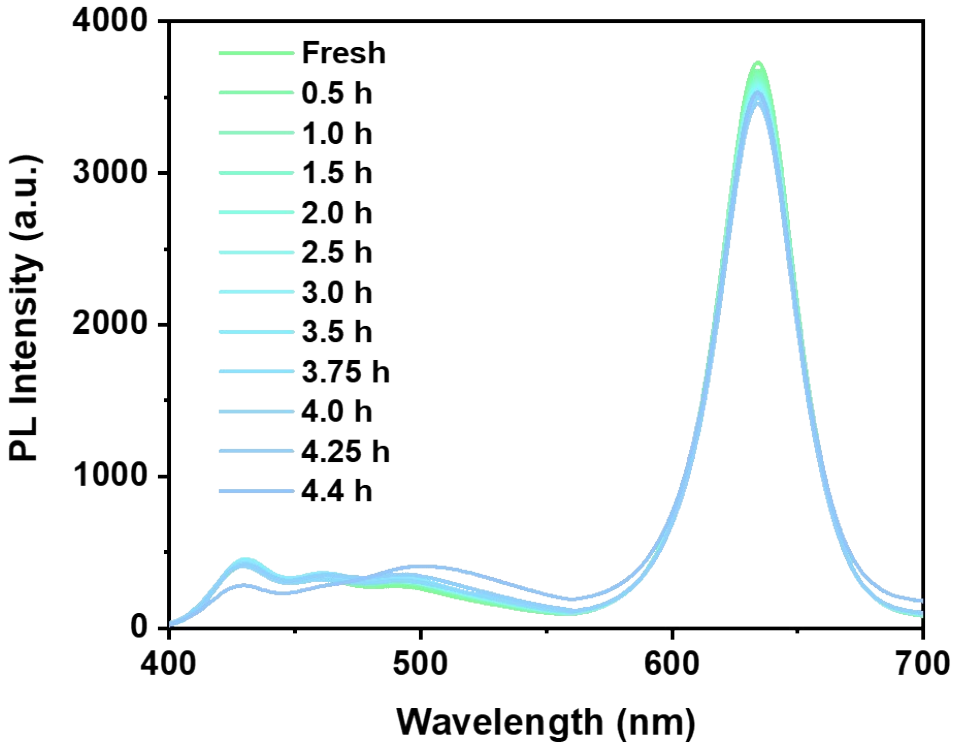

Figure S9. Time-dependent PL of QLEDs operating at constant current density.

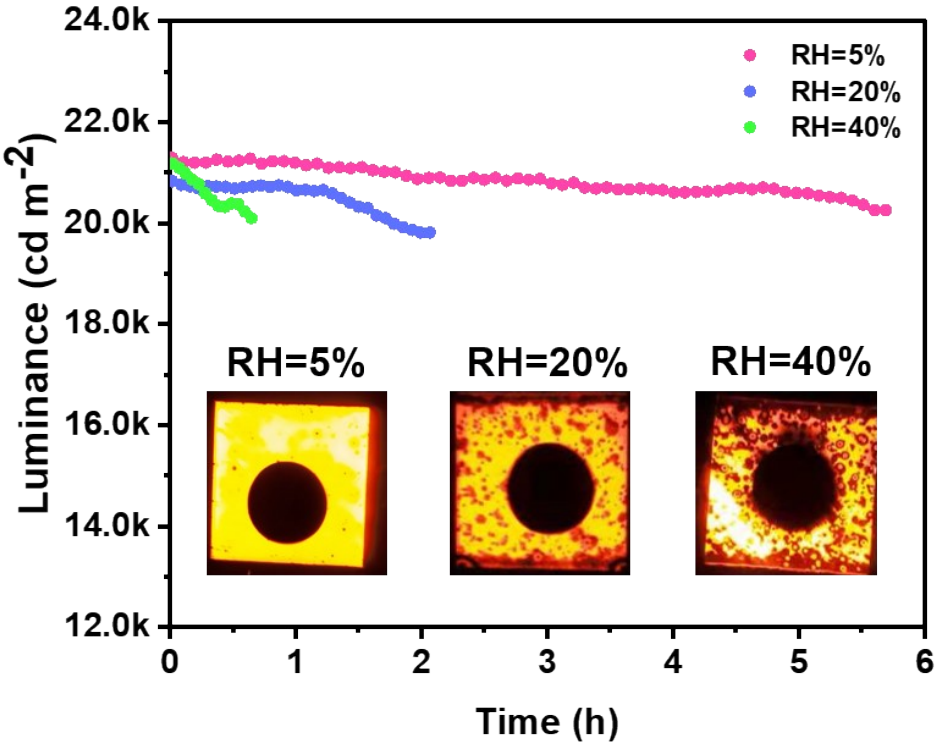

Figure S10. The stability of QLEDs operating at various humidity.

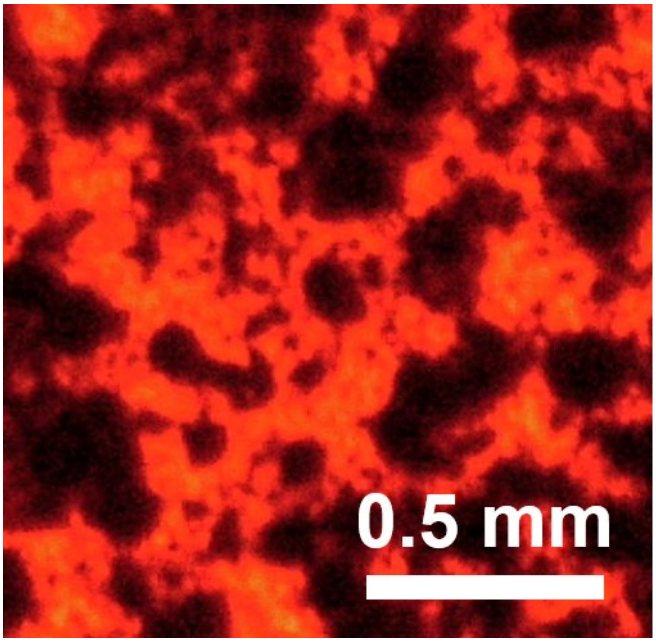

Figure S11. The fluorescent photograph of the reconstructed QLEDs.

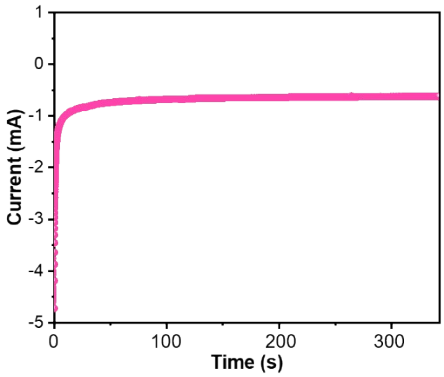

Figure S12. The I-t curve of electrochemical reduction of TFB film under constant voltage under -2 V.

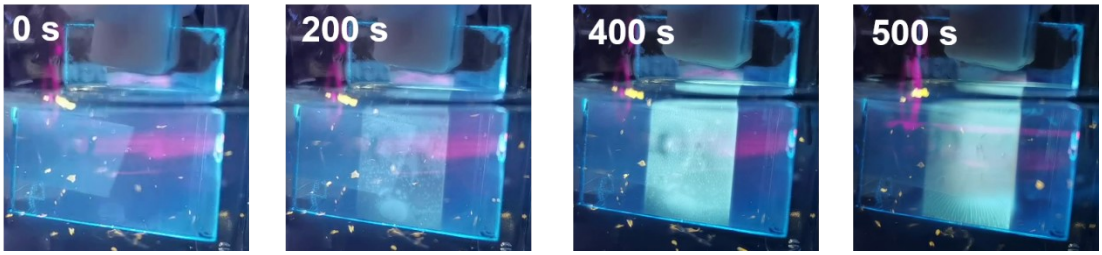

Figure S13. Fluorescence optical photograph of the WE during a steady reduction potential of -2 V.

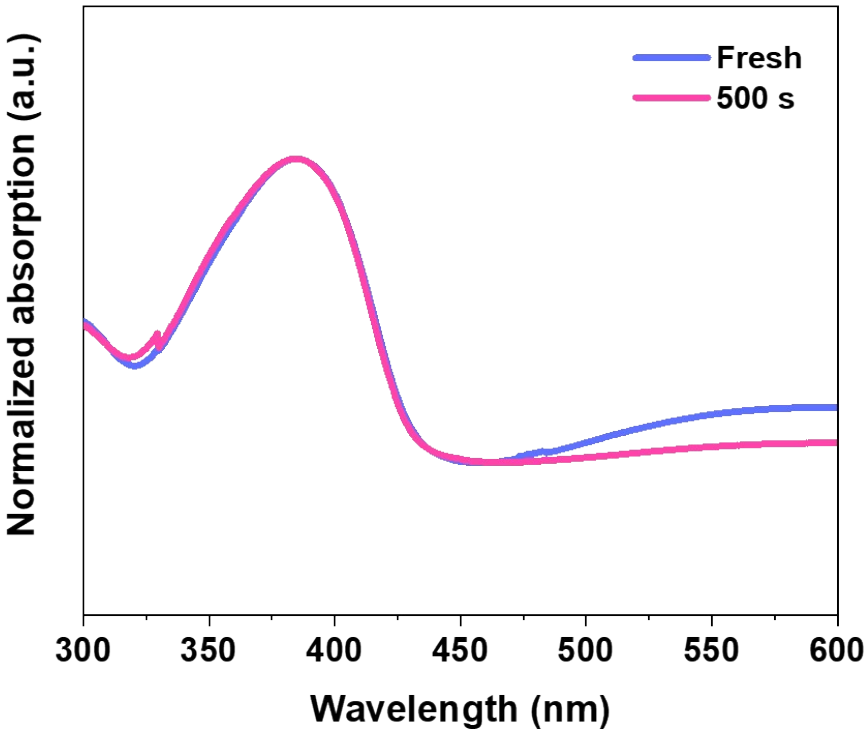

Figure S14. Absorption spectra of the TFB films before and after electrochemical reduction.

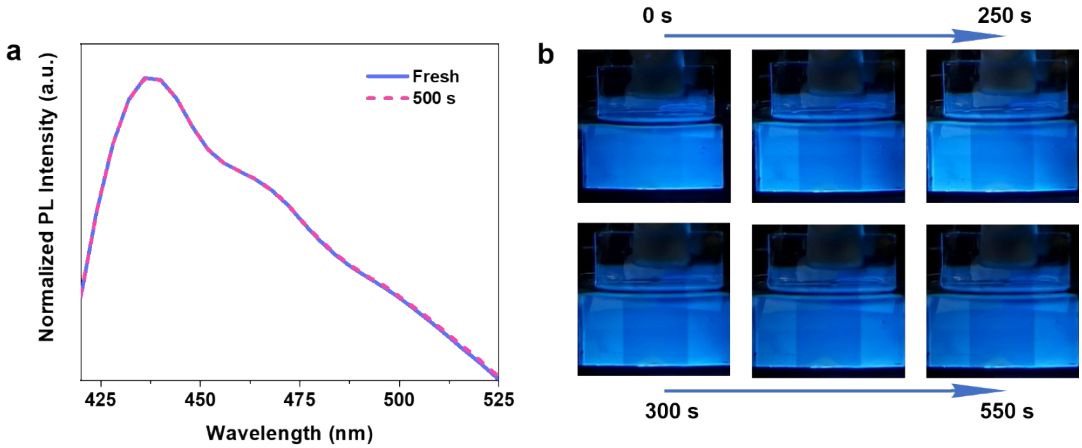

Figure S15. Optical characteristics of the TFB film after electrochemical oxidation. (a)PL spectra and (b) fluorescence optical photograph of the WE during a steady oxidation potential of 3 V.

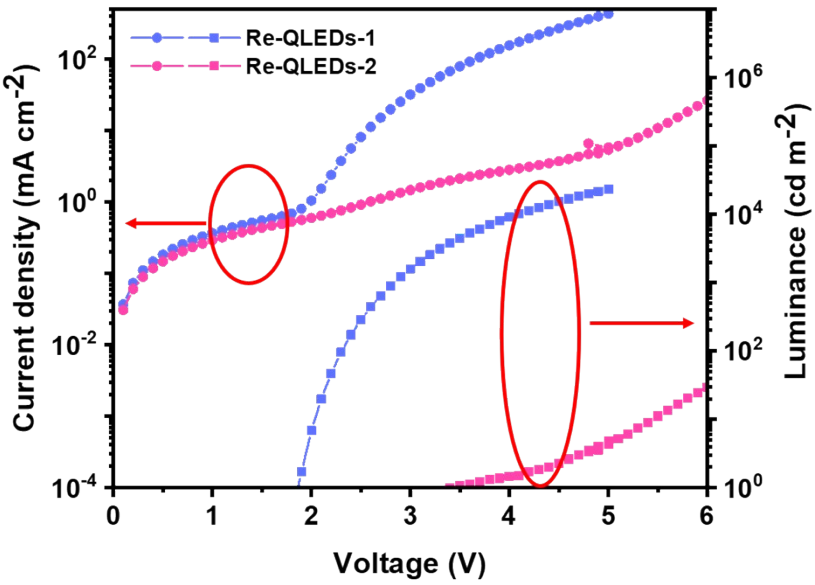

Figure S16. The current-voltage-luminance characteristics of Re-QLEDs.

4. The carrier transport properties of degraded TFB films was achieved by SCLC measurement.

The devices 1, 2, and 3 in **Figure 4a** had been operating for 0 h, 0.5 h, and 1 h, respectively. Thus, the TFB films with different degradation degree (different operation time) can be obtained after stripping ZnMgO and Ag electrodes of the devices. Then the QDs, MoO_3 and Ag were deposited successively on the TFB film to obtain HOD, which are named HOD-1, HOD-2, and HOD-3, respectively. Then obtained HOD was carried out the space-charge-limited-current (SCLC) measurement. The trap state densities (N_t) and carrier mobility can be estimated by SCLC measurement.[3-5] **Figure S13a**, **S13b**, and **S13c** present the SCLC curve of the HOD-1, HOD-2, and HOD-3, respectively. The curve can be divided into three sections, and exponential n is different. The n=1 at low bias voltage, indicating an ohmic contact response. The n=2 at high bias voltage is a trap-free region. The n>3 at medium bias voltage, is called trap-filled region.[4,5] The trap density N_t is calculated using the equation: [4,5]

$$N_t = \frac{2\varepsilon_0\varepsilon_r V_{TFL}}{ed^2} \quad (3)$$

where ε_0 and ε_r are the vacuum permittivity and the relative dielectric constant, respectively. V_{TFL} is the trap-filled limit voltage, and d is the thickness of the film. The V_{TFL} and N_t are 0.197 V and 8.5×10^{16} cm^{-3} for the HOD-1, 1.56 V and 6.7×10^{17} cm^{-3} for the HOD-2, and 2.02 V and 8.7×10^{17} cm^{-3} for the HOD-3, respectively (Table S2), meaning defect density increased significantly for the degraded TFB. The carrier mobility of TFB can be estimated from the J-V curve of the HOD by Mott-Gurney law:[5]

$$J_D = \frac{9\mu\varepsilon_0\varepsilon_r V_b^2}{8d^3} \quad (4)$$

Where J_D and V_b are the current density and applied voltage in the trap-free region, respectively. μ is the carrier mobility of the layer. From curve fittings, the hole mobility of HOD-1, HOD-2, and HOD-3 were calculated to be 5.79×10^{-6} cm^2 V^{-1} s^{-1}, 1.81×10^{-6} cm^2 V^{-1} s^{-1}, and 1.46×10^{-6} cm^2 V^{-1} s^{-1}, respectively.

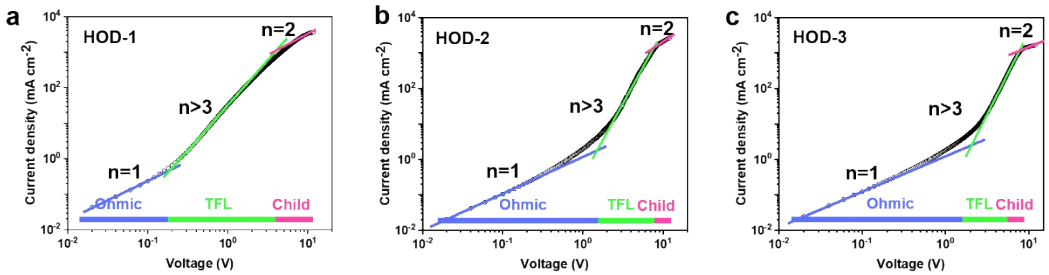

Figure S17. The carrier transport properties of degraded TFB. Space-charge-limited current of the (a) HOD-1, (b) HOD-2, and (c) HOD-3.

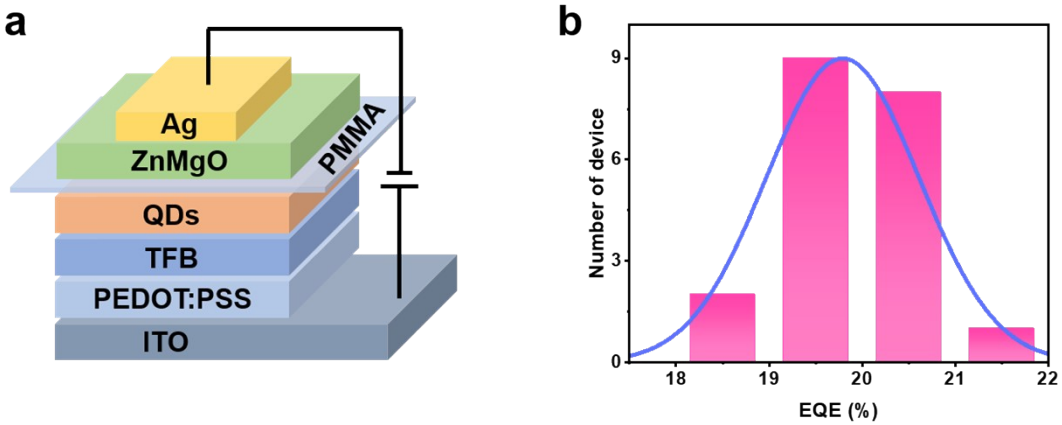

Figure S18. The performance of QLEDs with PMMA. (a) Device structure. (b) Histograms of the EQE.

Table S1. The Fitted Rs based on QLEDs with different degradation times.

	fresh	1.0 h	2.0 h	3.0 h	3.5 h	4.0 h	4.25 h	4.5 h
R_s (Ω cm^2)	4.5	6.3	6.7	12.3	17.9	22.8	33.6	80

Table S2. The fitted results through SCLC curve.

	V_{TFL} (V)	N_t (cm^{-3})	μ(cm^2 V^{-1} s^{-1})
HOD-1	0.197	8.5×10^{16}	5.79×10^{-6}
HOD-2	1.56	6.7×10^{17}	1.81×10^{-6}
HOD-3	2.02	8.7×10^{17}	1.46×10^{-6}

1. Chen, D.; Chen, D.; Dai, X.; Zhang, Z.; Lin, J.; Deng, Y.; Hao, Y.; Zhang, C.; Zhu, H.; Gao, F.; Jin, Y. Shelf-stable quantum-dot light-emitting diodes with high operational performance. *Adv. Mater.* **2020**, *32* (52), 2006178. DOI: 10.1002/adma.202006178
2. Ye, Y.; Zheng, X.; Chen, D.; Deng, Y.; Chen, D.; Hao, Y.; Dai, X.; Jin, Y. Design of the hole-injection/hole-transport interfaces for stable quantum-dot light-emitting diodes. *J. Phys. Chem. Lett.* **2020**, *11* (12), 4649-4654. DOI: 10.1021/acs.jpclett.0c01323
3. Li, R.; Wang, P.; Chen, B.; Cui, X.; Ding, Y.; Li, Y.; Zhang, D.; Zhao, Y.; Zhang, X. NiO_x/spiro hole transport bilayers for stable perovskite solar cells with efficiency exceeding 21%. *ACS Energy Lett*. **2020**, 5 (1), 79-86. DOI: 10.1021/acsenergylett.9b02112
4. Yuan, J.; Bi, C.; Wang, S.; Guo, R.; Shen, T.; Zhang, L.; Tian, J. Spray-coated colloidal perovskite quantum dot films for highly efficient solar cells, *Adv. Funct. Mater.* **2019**, *29* (49), 1906615. DOI: 10.1002/adfm.201906615
5. Kim, S.-K.; Yang, H.; Kim, Y.-S. Control of carrier injection and transport in quantum dot light emitting diodes (QLEDs) via modulating Schottky injection barrier and carrier mobility. *J. Appl. Phys.* **2019**, *126*, 185702. DOI: 10.1063/1.5123670